PNAS RESEARCH ARTICLE | MEDICAL SCIENCES CHEMISTRY

Dendrimer nanosystems for adaptive tumor-assisted drug delivery via extracellular vesicle hijacking

Yifan Jiang[a,b], Zhenbin Lyu[a], Brigino Ralahy[a], Juan Liu[a,c,d], Tom Roussel[a], Ling Ding[a], Jingjie Tang[a], Artemis Kosta[e], Suzanne Giorgio[a], Richard Tomasini[b], Xing-Jie Liang[c], Nelson Dusetti[b], Juan Iovanna[b], and Ling Peng[a,1]

Edited by Jonathan Sessler, The University of Texas at Austin, Austin, TX; received September 14, 2022; accepted January 4, 2023

Drug delivery systems (DDSs) that can overcome tumor heterogeneity and achieve deep tumor penetration are challenging to develop yet in high demand for cancer treatment. We report here a DDS based on self-assembling dendrimer nanomicelles for effective and deep tumor penetration via in situ tumor-secreted extracellular vesicles (EVs), an endogenous transport system that evolves with tumor microenvironment. Upon arrival at a tumor, these dendrimer nanomicelles had their payload repackaged by the cells into EVs, which were further transported and internalized by other cells for delivery "in relay." Using pancreatic and colorectal cancer-derived 2D, 3D, and xenograft models, we demonstrated that the in situ-generated EVs mediated intercellular delivery, propagating cargo from cell to cell and deep within the tumor. Our study provides a new perspective on exploiting the intrinsic features of tumors alongside dendrimer supramolecular chemistry to develop smart and effective DDSs to overcome tumor heterogeneity and their evolutive nature thereby improving cancer therapy.

dendrimer | adaptive drug delivery | Extracellular vesicles | supramolecular dendrimer nanomicelle | tumor-assisted drug delivery

Significance

Cancer is one of the leading causes of death in the world and remains a difficult disease to treat because of its intrinsic heterogeneity and dynamic evolution. The drug delivery system reported in this study was effective for drug delivery deep inside the tumor, leading to excellent anticancer activity. It exploits in situ tumor-secreted extracellular vesicles (EVs), an endogenous transport system that evolves with the parental cancer cells in the tumor microenvironment, hence overcoming tumor heterogeneity and dynamic evolution. These promising results highlight the remarkable potential of this drug delivery system for cancer treatment and provide a proof of concept for the development of new therapeutic modalities that exploit the intrinsic features of tumors for adaptive drug delivery.

Over the last few decades, nanotechnology-based drug delivery systems (DDSs) have been applied to improve drug efficacy in cancer treatment. However, the success rate of the clinical translation of nanomedicine remains extremely low (1). One key reason for this poor conversion is the inefficient intratumoral penetration of the DDSs, primarily due to the insufficient blood supply, abundant stroma, and high interstitial fluid pressure found within the tumor microenvironment (TME) (2, 3). Another critical concern is the heterogeneity and evolutive nature of tumors, which further compromise the treatment outcome (1, 4). Consequently, innovative and out-of-the-box strategies using smart delivery tools for effective and deep tumor penetration while overcoming tumor heterogeneity and dynamic evolution are urgently required.

Tumors can be considered as complex "organs" comprising multiple dynamic cellular and acellular barriers (5). The tumor "organs" can evolve and refresh these barriers during their progression and in response to cancer treatment (6). Importantly, however, while the heterogeneous intratumoral barriers constantly evolve to hinder exogenous DDSs, the tumor always maintains open "gateways" for endogenous delivery systems allowing entry to necessary nutrients, growth factors, and signaling molecules for growth and proliferation. Without these "gateways," the tumor would experience self-limitation and self-eradication.

Among the various endogenous delivery systems, extracellular vesicles (EVs) are of particular importance for tumors. EVs are nano- and micro-sized vesicles that are secreted by almost all cell types (7) and that can load various cargos including endogenous proteins and nucleic acids, as well as exogenous materials. They serve as intercellular delivery systems for the transport of materials and signaling molecules (8, 9). Crucially, EVs are evolutionarily conserved, while being over-produced in tumors (10). EVs generated in situ within tumors bear and maintain the heterogeneous and evolutive features of their parental cells (8, 11, 12). In particular, the transport and penetration of tumor-secreted EVs can be facilitated by the tumor extracellular matrix, which otherwise obstructs exogenous materials (13, 14). Therefore, such EVs generated in situ within tumors constitute ideal DDSs able to adapt to the heterogeneous and evolving TME and simultaneously allow deep tumor penetration for effective cancer treatment.

We have been actively engaged in advancing dendrimer-based nanosystems for drug delivery in cancer therapy. Dendrimers, a special class of polymers with radially symmetric and well-defined structures, have emerged as high-precision vectors in drug delivery by virtue of their precisely controllable structure and cooperative multivalence (15–18). With the aim of harnessing the unique structural properties of dendrimers and the self-assembling feature of lipids (19–22) to develop a nanotechnology-based DDS, various amphiphilic

Author contributions: Y.J. and L.P. designed research; Y.J., Z.L., B.R., J.L., T.R., L.D., J.T., A.K., and S.G. performed research; Z.L., B.R., N.D., and J.I. contributed new reagents/analytic tools; Y.J., J.L., T.R., R.T., X.-J.L., N.D., J.I., and L.P. analyzed data; and Y.J., T.R., and L.P. wrote the paper.

The authors declare no competing interest.

This article is a PNAS Direct Submission.

[1]To whom correspondence may be addressed. Email: ling.peng@univ-amu.fr.

This article contains supporting information online at https://www.pnas.org/lookup/suppl/doi:10.1073/pnas.2215308120/-/DCSupplemental.

Published February 6, 2023.

dendrimers (ADs), which can self-assemble into nanovesicles and/or nanomicelles, have been established (23–30). We have recently developed amphiphilic poly(amidoamine) (PAMAM) dendrimer nanomicelles (ADNMs) for drug delivery (31, 32). Here, we demonstrate that these uniquely smart ADNM-based DDSs exploit EVs generated in situ within tumors for drug delivery. Hijacking these EVs enables an enhanced intratumoral transport of the ADNM payload allowing its deep tumor penetration while overcoming tumor heterogeneity and dynamic evolution (Fig. 1). Specifically, ADNMs first home in onto the tumors via the enhanced permeability and retention (EPR) effect. Upon uptake by both tumor and stromal cells, the payload of the ADNMs is repackaged into EVs, and EV-mediated intercellular delivery is promoted. The secreted EVs are then further transported deeper inside the tumor and internalized by other cells for drug delivery "in relay," which is facilitated by the passage offered by the TME (Fig. 1). This sequential process of in situ payload repackaging into EVs, combined with subsequent EV transport and cellular uptake, enabled the continuous propagation of drug from cell to cell and achieved deep penetration inside tumors. Importantly, the exploitation of the tumor-produced EVs overcame the problems commonly facing drug delivery associated with tumor heterogeneity and dynamic evolution of the TME. This study highlights the great potential of exploiting the intrinsic features of tumors alongside dendrimer supramolecular chemistry to develop smart and effective DDSs for cancer therapy. Below, we present our results using pancreatic and colorectal cancer-derived 2D, 3D, and xenograft models to demonstrate ADNM-mediated intratumoral drug delivery deep inside tumor tissue, leading to the effective inhibition of tumor growth while obviating the side effects.

Results and Discussion

Anticancer Efficacy and Deep Tumor Penetration. We previously developed the AD (Fig. 2*A*) which self-assembled into nanosized micelles and successfully encapsulated the anticancer drug doxorubicin (DOX).(32) In the present study, we revealed that AD can also encapsulate other anticancer drugs, including paclitaxel (PTX)(17) and rapamycin (R) (also an immunosuppressant [33)] (Fig. 2*A*). While these anticancer drugs display potent anticancer activity, they also exhibit distinct toxicities and side effects which compromises their therapeutic efficacy in patients. DDSs are therefore required to overcome these limitations and enable the wide use of these drugs in cancer treatment. It should be mentioned that although DOX, PTX, and R have markedly different chemical structures, their ADNMs—denoted DOX/AD, PTX/AD, and R/AD, respectively—all exhibited high drug loading (29 to 39%) and encapsulation efficiency (85 to 99%), and measured 12 to 20 nm in size (Fig. 2*B* and *SI Appendix*, Table S1). These results highlight the wide scope and general interest in ADNM-based DDSs for encapsulating various structurally diverse drugs.

Notably, all of the prepared ADNMs (DOX/AD, PTX/AD, and R/AD) displayed excellent anticancer activity with a significant inhibition of tumor growth in the PDAC087T and

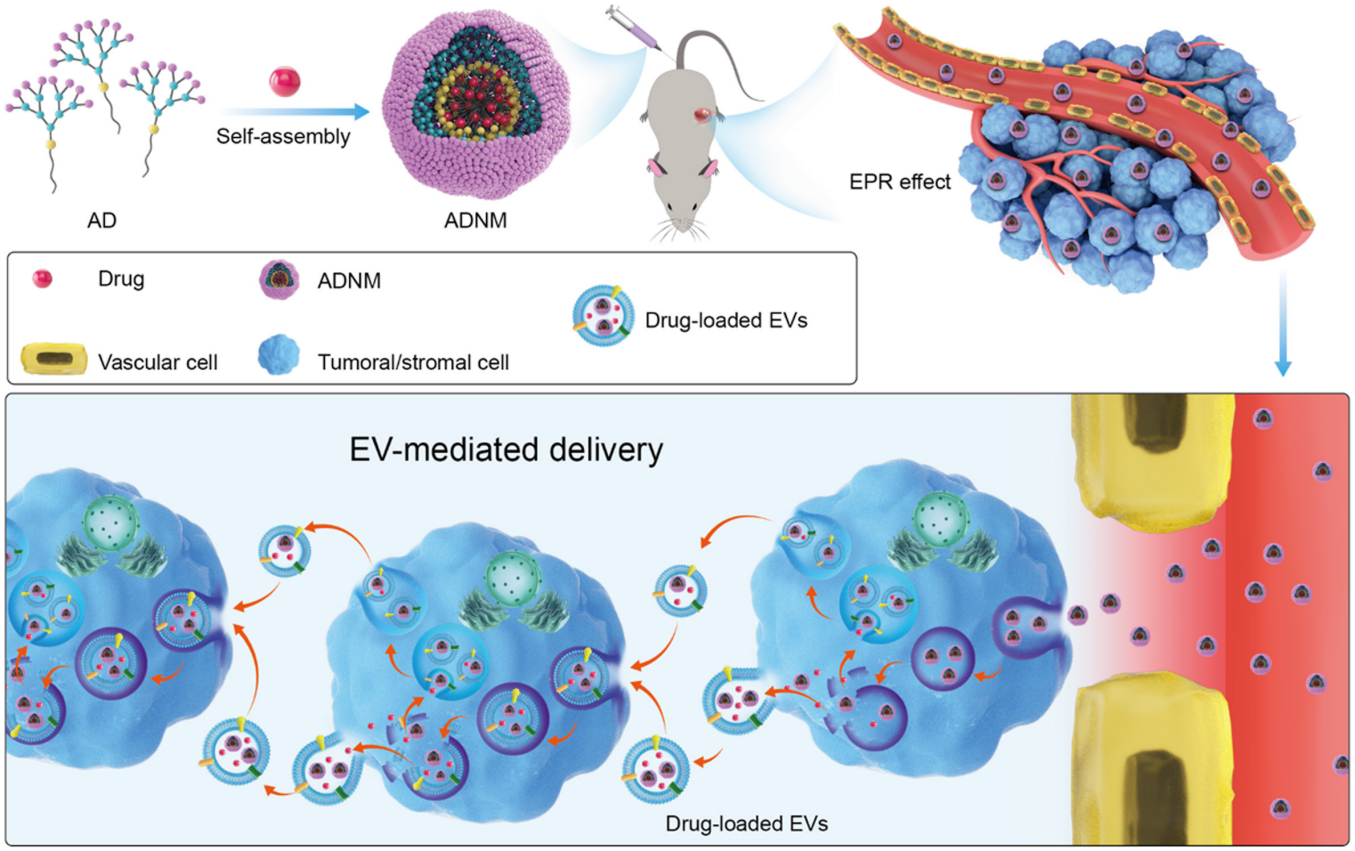

Fig. 1. ADNMs Encapsulate the Anticancer Drug and Induce Tumor-Assisted Drug Delivery via EV-Mediated Intercellular Transport. The amphiphilic dendrimer (AD) encapsulates the anticancer drug and forms nanomicelles (ADNMs) which reach the tumor lesion via the EPR effect. There they induce in situ tumor-assisted drug delivery for deep tumor penetration via EV-mediated intercellular transport. This EV-mediated delivery process involves: 1) internalization of ADNMs inside cells within the tumor tissue; 2) repackaging of ADNM payload into EVs; 3) intercellular transport of the generated EVs; 4) internalization of the generated EVs by the recipient cell.

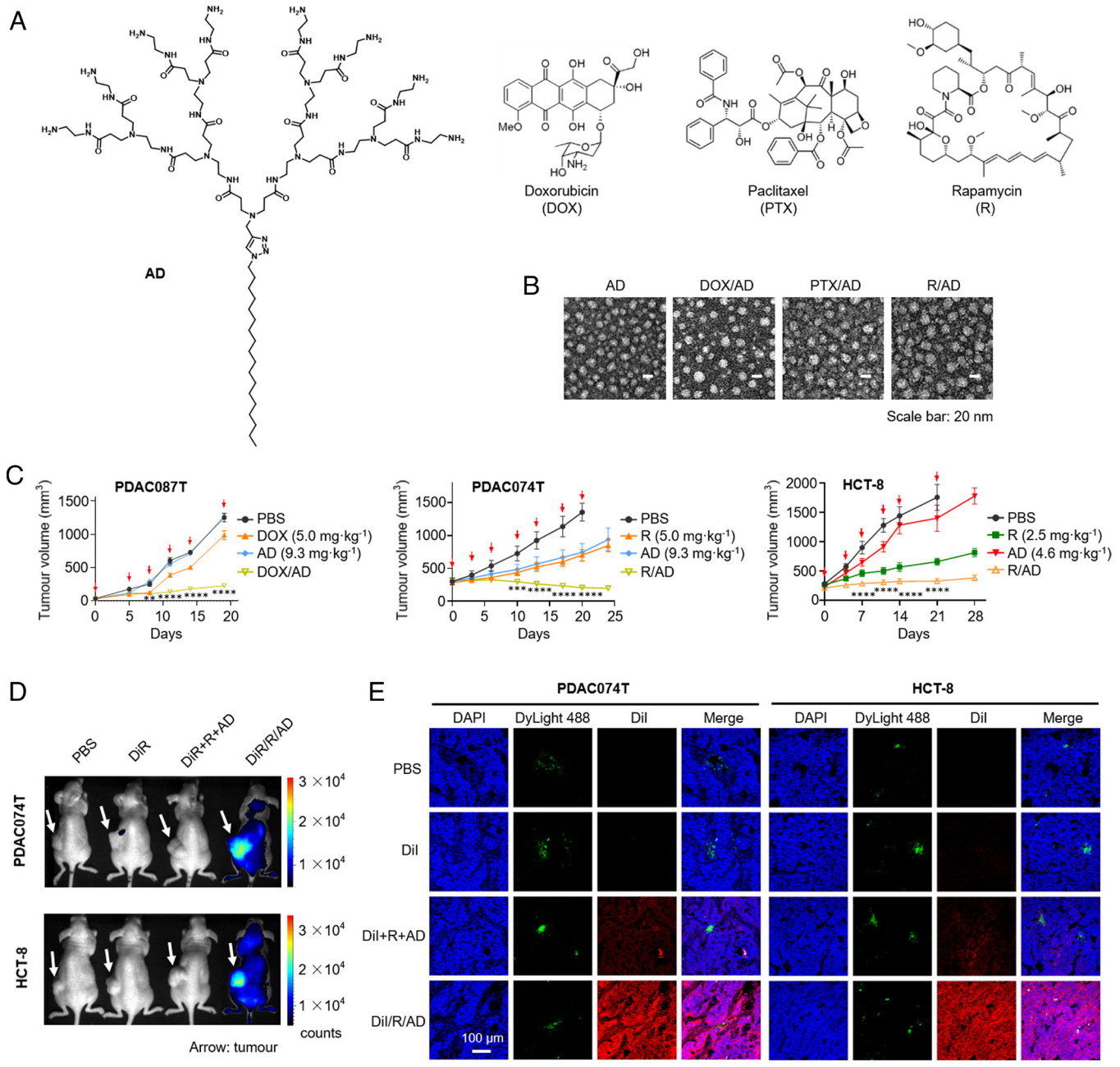

Fig. 2. ADNMs Were Effective for Drug Delivery and Inhibiting Tumor Growth via Specific Accumulation and Deep Penetration in Tumor. (*A*) Chemical structure of the AD, and the anticancer drugs DOX, PTX and R used in this study. (*B*) Small and spherical nanoparticles of the ADNM-based DDSs observed under transmission electron microscope (TEM). DOX/AD, PTX/AD and R/AD refer to DOX-, PTX- and R-loaded ADNMs, respectively. (*C*) Tumor growth curves of the patient-derived pancreatic cancer xenografts PDAC087T and PDAC074T, and the colorectal cancer HCT-8 xenografts in mice upon treatment with DOX/AD and R/AD, respectively. Mice treated with PBS buffer, drug alone or dendrimer alone were used as the controls. Data are presented as the mean ± SEM. The statistical significance was calculated by two-way ANOVA with a Tukey's multiple comparisons test. n = 6 mice for all groups. $^{*}P < 0.05$, $^{**}P < 0.01$, $^{***}P < 0.001$, $^{****}P < 0.0001$. (*D*) Accumulation of R/AD in tumors in the PDAC074T and HCT-8 xenograft mice was analyzed using fluorescent imaging with ADNM carrying both rapamycin and the near-infrared fluorescent dye DiR (DiR/R/AD). The in vivo fluorescence images were acquired 48 h after intravenous administration of DiR/R/AD in PDAC074T (*Upper*) and HCT-8 (*Lower*) xenografts. Mice treated with PBS, free DiR, and a simple mixture of DiR, rapamycin and AD (DiR + R + AD), were used as controls. Arrows point to the tumor locations. (*E*) Confocal images of tumor tissues show a deep intratumoral penetration of R/AD, using ADNM loaded with both rapamycin and the fluorescent dye DiI (DiI/R/AD). Mice treated with PBS, DiI alone, or a simple mixture of DiI, rapamycin and AD (DiI + R + AD), were used as controls. Tumors were harvested from PDAC074T (*Left*) and HCT-8 (*Right*) xenografts 24 h post-intravenous administration, then cryosectioned and imaged by tracing DiI fluorescence (red). Blood vessels were labelled with DyLight488-labeled Lycopersicon esculentum lectin (green), and nuclei with DAPI (blue).

PDAC074T patient-derived pancreatic cancer xenograft models, as well as in the HCT-8 colorectal cancer model (Fig. 2*C* and *SI Appendix*, Fig. S1 *A* and *B*). Co-encapsulation of the near-infrared fluorescent dye DiR in ADNMs allowed us to confirm their effective accumulation within the tumor lesions (Fig. 2*D* and *SI Appendix*, Fig. S2*A*). This can be attributed to the EPR effect in the TME, where the leaky vasculature and dysfunctional lymphatic drainage enables passive tumor targeting (34–36).

Further fluorescence imaging of the tumor tissue from mice treated with DiI/R/AD (Rapamycin co-formulated with the fluorescent dye DiI in ADNMs) illustrated that the DiI fluorescence signal (red) was uniformly distributed throughout the entire tumor

section, and the fluorescence intensity was much higher in the DiI/R/AD-treated mice group than in the control groups treated with DiI or DiI + R + AD (a simple mixture of DiI, R, and AD) in both PDAC074T and HCT-8 tumors (Fig. 2*E* and *SI Appendix*, Fig. S2*B*). These data demonstrate the capacity of ADNMs to penetrate deep within the tumor, using a mechanism which is independent of tumor permeability, as shown by their ability to penetrate both the poorly permeable PDAC074T model and the highly permeable HCT-8 tumor model (Fig. 2*E* and *SI Appendix*, Fig. S3) (37). This particularly advantageous feature offered by ADNMs thus helped overcome the heterogeneous features of tumors, allowing effective and deep intratumoral delivery.

EV Cargo Loading and Cellular Uptake. The promising anticancer activity and deep tumor penetration shown by ADNMs motivated us to evaluate the mechanism underlying their delivery. We therefore studied whether the intratumoral delivery and penetration of ADNMs were mediated by EVs generated in situ in tumors. We first investigated the influence of ADNMs on the key steps that would be associated with EV-mediated intercellular drug delivery (38–42)—payload repackaging into EVs and subsequent cellular uptake of EVs—using cell-based experiments.

To facilitate the study on EV cargo loading and cellular uptake using fluorescence imaging, we used rapamycin as the model drug and co-encapsulated it with the fluorescent dye Cy3 in ADNMs. The Cy3/R-coloaded ADNMs (C/R/AD) as well as ADNMs co-loaded with other fluorescent dyes DiI and DiR (DiI/R/AD and DiR/R/AD, respectively), exhibited similar size and morphology to R-loaded ADNMs (R/AD) (*SI Appendix*, Fig. S4).

EVs generated from cells pretreated with ADNMs were collected using previously reported protocols (43, 44) and grouped as small (SEVs) and large EVs (LEVs) according to their size. They exhibited the characteristic size and morphology of EVs (Fig. 3 *A*–*C*) and retained the EV markers TSG101, CD81, and CD9 (Fig. 3*D*). Using flow cytometry, we assessed cargo loading in the EVs generated by cancer cells PDAC074T and HCT-8 as well as stromal cells CAFi (a cancer-associated fibroblast cell line) and L929 (a normal fibroblast cell line) upon treatment with C/R/AD or a control, either Cy3 alone or Cy3 simply mixed with R (C+R), AD (C+AD), or both (C + R + AD, Fig. 3 *E*–*H* and *SI Appendix*, Fig. S5). Our results revealed significantly higher Cy3 fluorescence intensity in both LEVs and SEVs generated in the C/R/AD group compared to those in any of the control groups. Indeed, although C + R enhanced the Cy3 content in EVs, it was much less efficient than C/R/AD. The Cy3-loaded EVs generated with the simple mixture (C + R + AD) showed a significantly lower fluorescence intensity than those prepared with C/R/AD, highlighting the importance of the nanoformulation with AD in the observed enhanced payload packaging into EVs.

The capacity of ADNMs to enhance EV loading with exogenous cargo was also confirmed using DOX-loaded ADNMs (DOX/AD). The DOX fluorescence signal of EVs generated with DOX/AD was much more intense than that resulting from treatment with DOX alone or a mixture of DOX and AD (DOX + AD, *SI Appendix*, Fig. S6). Collectively, these results indicate that EV cargo loading was significantly promoted by ADNMs and that the observed enhancement was highly nanoformulation dependent and not payload dependent.

We further demonstrated that the cargo-loaded EVs were readily internalized by recipient cells. Incubating recipient cells (PDAC074T) with both LEVs and SEVs generated by donor PDAC074T cells treated with C/R/AD led to the detection of Cy3 signals in the recipient cells (Fig. 3 *I* and *J*). Moreover, the cellular uptake of EVs was enhanced upon treatment of PDAC074T and HCT-8 cells with R/AD (Fig. 3 *K* and *L*), highlighting the active role played by ADNMs. Together, these results demonstrate that ADNM not only promotes cargo repackaging into EVs but also the uptake of these EVs by recipient cells, and thereby provide evidence of their potential for use as intercellular transport systems in drug delivery.

EV-Mediated Intercellular Delivery and Deep Tumor Penetration. To assess the intercellular delivery of in situ-generated and loaded EVs between cells, we first studied the transport of the loaded EVs in vitro using confocal microscopy (Fig. 4 and *SI Appendix*, Fig. S7). In order to allow easy distinction in confocal imaging, cells were prestained with either CFSE (green) or CellTrace™ Violet (blue). EVs (Fig. 4*B*, *Upper*) secreted by PDAC074T cells (CFSE-prestained, green) treated with C/R/AD were found to be intercellularly transported into the CellTrace™ Violet (blue) prestained PDAC074T cells (Fig. 4*B*, *Middle* and *Lower*) and vice versa by tracing EVs exhibiting both green (CFSE) and red (Cy3) fluorescence. Similar results were also observed with cocultured HCT-8 cells prestained with CFSE and CellTrace™ Violet (Fig. 4*C*). Remarkably, this EV-mediated intercellular delivery was also observed between cocultured tumor and stromal cells, as revealed by cocultured PDAC074T/CAFi (Fig. 4*D*), HCT-8/CAFi (Fig. 4*E*), and PDAC074T/L929 cells (Fig. 4*F*). Similar results were obtained in prestained cells treated with C/PTX/AD (co-formulation of paclitaxel and the fluorescent dye Cy3 within ADNM, *SI Appendix*, Fig. S7). These data indicate that the ADNM payload was repackaged into EVs by both tumor and stromal cells and delivered via EV-mediated transport from cell to cell. These observations agree with those obtained by flow cytometry (Fig. 3 *E* and *I* and *SI Appendix*, Fig. S8).

To investigate whether cargo-loaded EVs can serve as an intercellular delivery system for deep tumor penetration, we used 3D spheroid models to mimic the TME, which often has abundant stroma and over-crowded cancer cells confined within a 3D space. We first examined the penetration of C/R/AD into spheroids using two-photon microscopy. Fluorescence imaging revealed much stronger and deeper penetration of C/R/AD into spheroids of PDAC074T (Fig. 5*A*) and co-cultured PDAC074T/L929 cells (Fig. 5*B*) than those observed for all of the controls. Similar results were obtained with DOX/AD and C/PTX/AD (*SI Appendix*, Fig. S9 *A* and *B*). Collectively, these results demonstrate that ADNMs effectively assisted delivery and enhanced its efficiency by enabling deep tumor penetration.

To investigate the role of EV-mediated delivery in the observed deep penetration in spheroids, we then tested the effect of GW4869 (an EV genesis inhibitor), cytochalasin D (CytoD, an inhibitor of EV genesis and uptake), (45, 46) blebbistatin [Bleb, an EV formation inhibitor (47)], and methyl-β-cyclodextrin [mβCD, an EV uptake inhibitor (48)] on the spheroid penetration observed with C/R/AD. We also used EXO1, an inhibitor of exocytosis, (49) a nanoparticle transport-associated pathway, as the control. Fluorescence imaging revealed that the penetration of C/R/AD and C/PTX/AD into the spheroids was greatly hindered by GW4869, CytoD, Bleb, and mβCD, but not by EXO1 (Fig. 5 *C* and *D* and *SI Appendix*, Fig. S9 *C*–*E*), confirming the role of EV-mediated intratumoral delivery and penetration. Altogether, these results confirm that the observed penetration of ADNMs into tumor spheroids was associated with EV-mediated intercellular transport.

To further support these findings, we inspected tumor tissues obtained from xenograft mice. Specifically, tumors were collected from HCT-8GFP xenograft mice after intravenous administration of the fluorescently labeled nanomicelle system

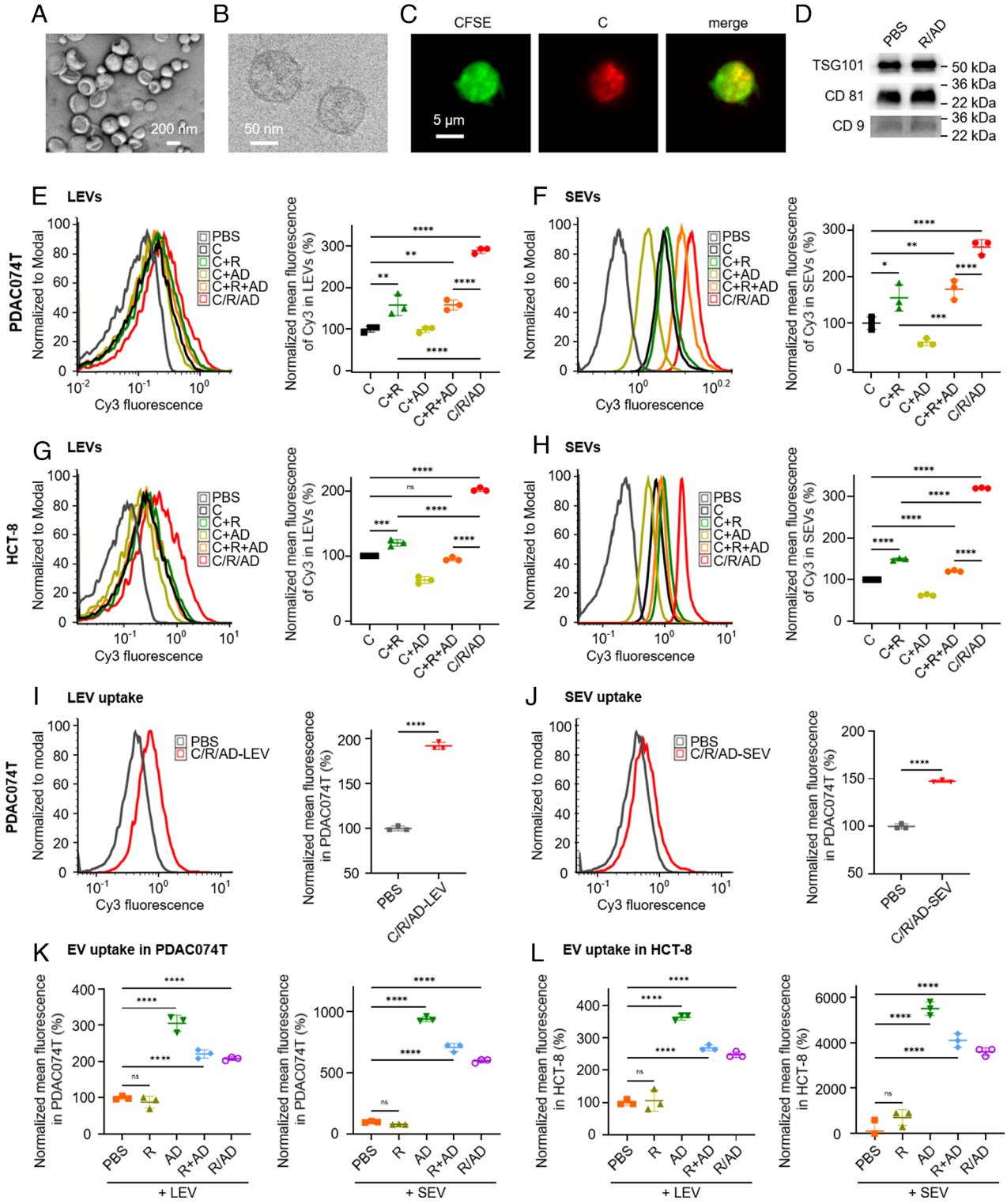

Fig. 3. ADNM Induced EV Payload-Packaging and Cellular Uptake. (*A–D*) EVs, generated by cells upon treatment with ADNM, were characterized using TEM, cryogenic electron microscopy (Cryo-EM), fluorescent microscopy and biomarkers. TEM (*A*) and Cryo-EM (*B*) images of EVs generated by PDAC074T pretreated with R/AD; Fluorescent images of LEVs generated by CellTrace™CFSE-prestained PDAC074T pretreated with C/R/AD (*C*); EVs derived from PDAC074T cells upon treatment with R/AD retained the same EV markers: TSG101, CD81, and CD9, as those generated in the control group in PBS. EV markers were revealed using western blotting (*D*). (*E–H*) Payload-packaging in EVs generated by the cancer cells PDAC074T upon treatment with C/R/AD (co-formulation of the fluorescent Cy3 and rapamycin within ADNM) was studied using flow cytometry. The Cy3-positive LEVs (*E* and *G*) and SEVs (*F* and *H*) generated by PDAC074T and HCT-8 cells, respectively, were quantified using flow cytometry and presented in a histogram (*Left*) and normalized mean fluorescence (*Right*), with the free Cy3, the mixture of Cy3 and R (C + R), the mixture of Cy3 and AD (C + AD), and the mixture of Cy3, R and AD (C + R + AD) as the controls. (*I* and *J*) The uptake of the cargo-packaged EVs in recipient cells. Flow cytometrical analysis revealed that the recipient PDAC074T cells were Cy3-positive after incubation with, respectively, LEVs (*I*) and SEVs (*J*) generated from the donor PDAC074T cells pretreated with C/R/AD. Results are presented in a histogram (*Left*) and in normalized mean fluorescence (*Right*). (*K* and *L*) Uptake of the CellTrace™Yellow-labelled EVs in the recipient cells PDAC074T (*K*) and HCT-8 (*L*) was further enhanced upon treatment with AD, R + AD, and R/AD but not R. Data are presented as the mean ± SD. The statistical significance was calculated by two-tailed Student's *t* test for comparison between two groups or one-way ANOVA with a Tukey's multiple comparison test for three or more independent groups. n = 3 for all groups; ns not significant; **P* < 0.05, ***P* < 0.01, ****P* < 0.001, *****P* < 0.0001.

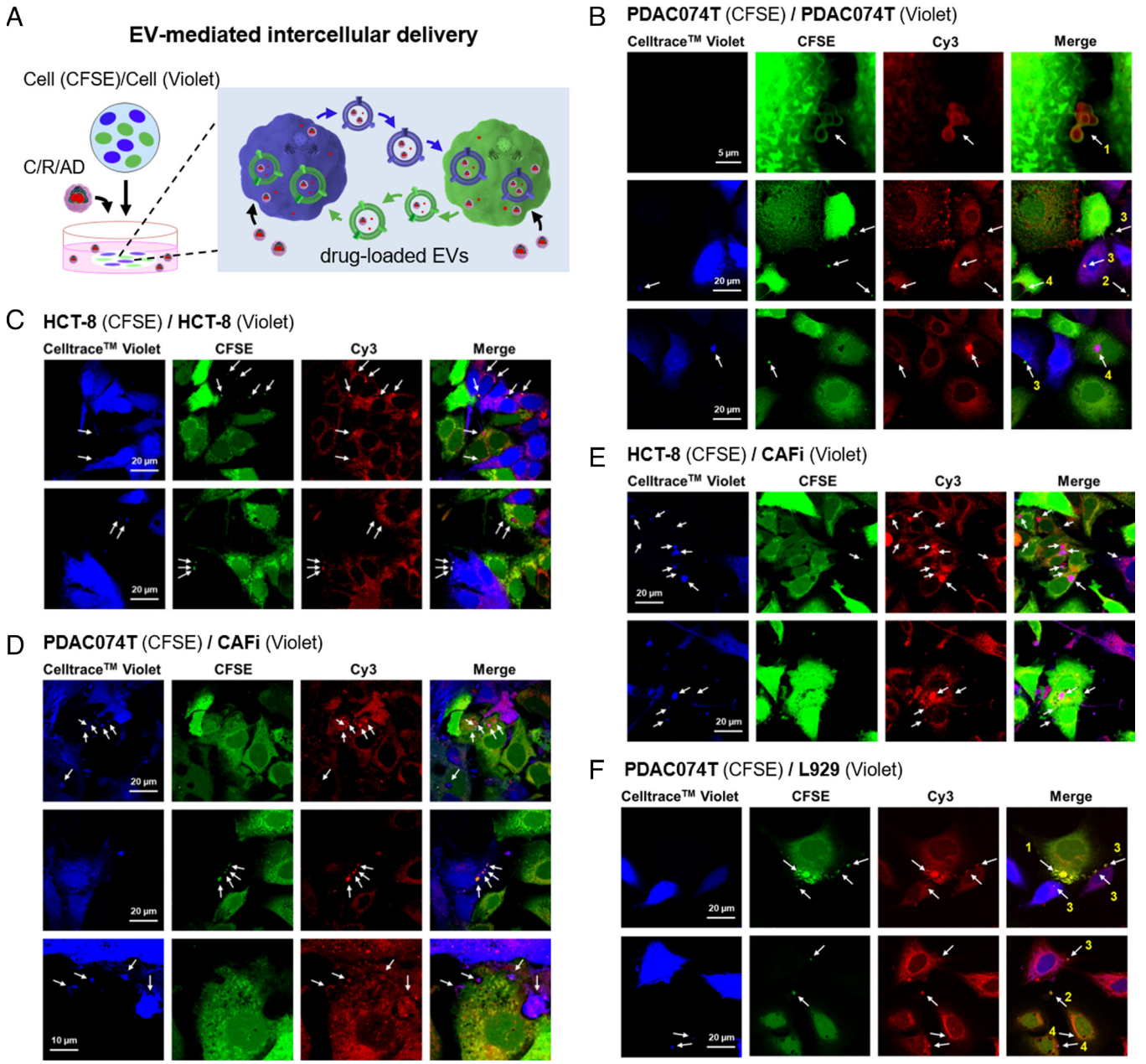

Fig. 4. Intercellular Delivery of Cargo-Loaded EVs. (*A*) Cartoon illustration of the intercellular delivery of cargo-loaded EVs studied using confocal imaging. Cells were prestained with either CFSE (green) or CellTrace™ Violet (blue) to allow easy distinction in confocal imaging. (*B–F*) Confocal imaging revealed that Cy3-loaded EVs were transported between cells in the co-culture of PDAC074T (CFSE, green) / PDAC074T (CellTrace™ Violet, blue) (*B*), HCT-8 (CFSE, green) / HCT-8 (CellTrace™ Violet, blue) (*C*), PDAC074T (CFSE, green) / CAFi (CellTrace™ Violet, blue) (*D*), HCT-8 (CFSE, green) / CAFi (CellTrace™Violet, blue) (*E*) and PDAC074T (CFSE, green) / L929 (CellTrace™ Violet, blue) (*F*), after incubation with C/R/AD. CAFi and L929 denote cancer-associated fibroblast and normal fibroblast, respectively. Arrows point to the Cy3-loaded EVs and show for example in *B* and *F*, arrows 1, the EVs (green) released by the green PDAC074T cells (CFSE) with Cy3-fluorescence (red) localized in their interior; arrows 2, the release of EVs (green) bearing Cy3 fluorescence from the green PDAC074T cells (CFSE) into the intercellular space; arrows 3, the Cy3-loaded EVs (green) released by the green PDAC074T cells (CFSE) and taken up by the blue PDAC074T cells (CellTrace™ Violet); arrows 4, the Cy3-loaded EVs (blue) released by the blue PDAC074T cells (CellTrace™ Violet) and taken up by the green PDAC074T cells (CFSE).

DiI/R/AD. HCT-8GFP cells allow visualization of the secreted EVs containing the hydrophilic GFP, (50) while DiI is a hydrophobic fluorescent dye (51) that only exhibits intense red fluorescence in hydrophobic environments such as the lipid bilayer of biomembranes and the central core of the ADNMs. Confocal imaging of tumors obtained from HCT-8GFP xenograft mice after treatment with DiI/R/AD revealed particles bearing a green (GFP) core and red (DiI) shell (Fig. 5*E*, arrows). These particles represented EVs derived from HCT-8GFP cells and loaded with DiI, and they were detected in the extracellular space (Box 1, Fig. 5*E*) and on the cell surface (Box 2, Fig. 5*E*) and edge (Box 3, Fig. 5*E*), as well as in the cytoplasm (Box 4, Fig. 5*E*). Notably, the EVs detected in Boxes 1 to 4 in Fig. 5*E* illustrate the entire process of EV-mediated intercellular delivery within the tumor: the DiI-loaded EVs were released into the intercellular space (Box 1, Fig. 5*E*) before adhering to the cell surface (Box 2, Fig. 5*E*) for internalization (Box 3, Fig. 5*E*) and entry into the cell (Box 4, Fig. 5*E*). These results are in line with those obtained using cell-based 2D and 3D models, confirming that ADNMs induced in situ-generation of EVs, in turn allowing the transport and propagation of the delivery cargo deep within the tumor.

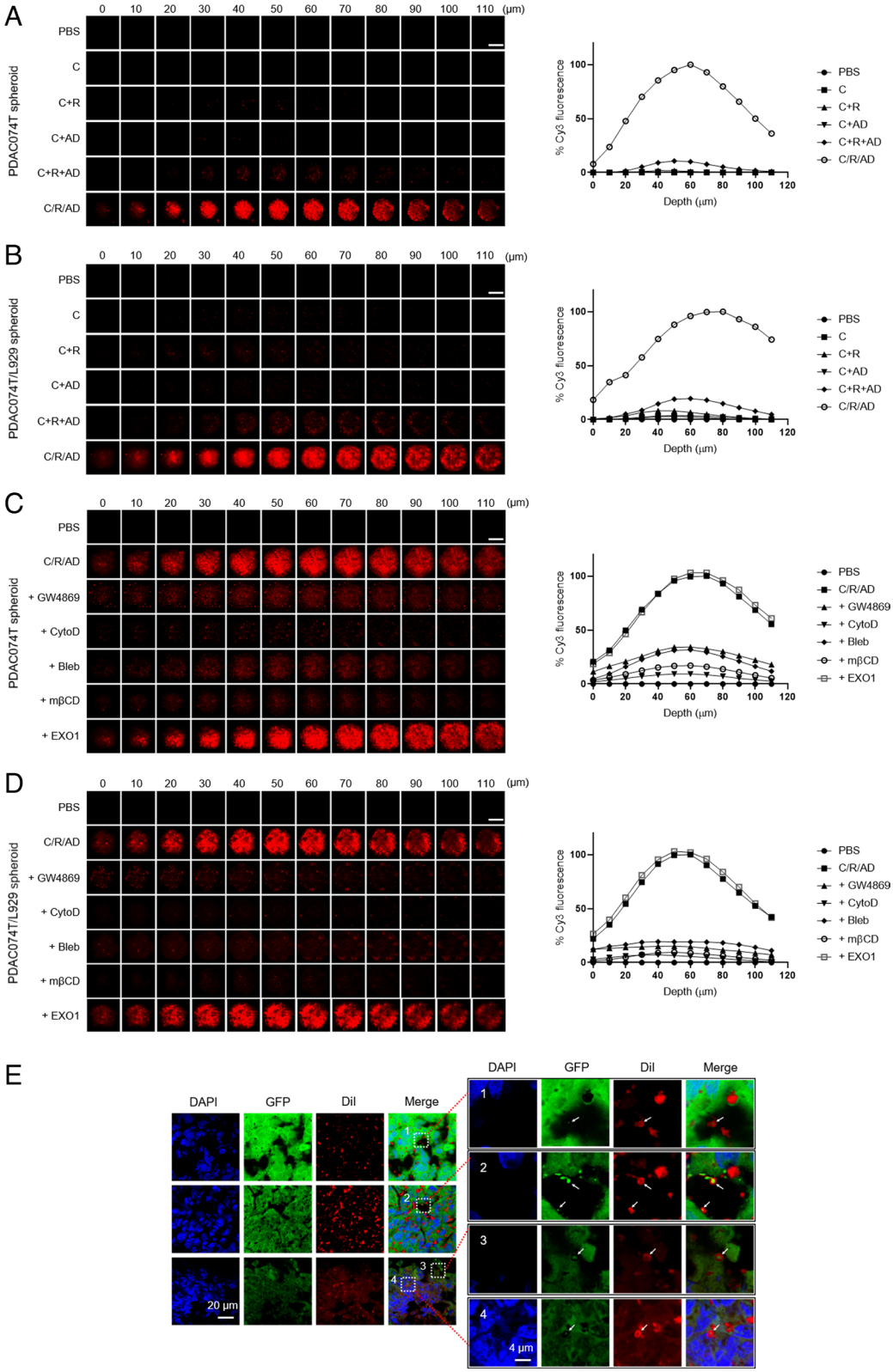

Fig. 5. Deep Penetration of ADNM Was Allowed via EV-Mediated Delivery in Spheroids and Tumors. (*A* and *B*) Deep penetration of C/R/AD in 3D spheroids constructed with PDAC074T cells (*A*) and co-cultured PDAC074T/L929 cells (*B*), was revealed by tracing the Cy3 fluorescence (red) using two-photon fluorescent microscopy, in comparison with the controls of Cy3 (C) alone, the mixture of Cy3 and R (C+R), the mixture of Cy3 and dendrimer AD (C + AD), and the mixture of Cy3, R and dendrimer (C+R+AD). (*C* and *D*), Penetration of C/R/AD in PDAC074T (*C*) and PDAC074T/L929 (*D*) spheroid was inhibited by the EV-genesis inhibitor GW4869 (20 μM), the EV-genesis and engulfment inhibitor cytochalasin D (CytoD, 1.0 μM), the EV-formation inhibitor blebbistatin (Bleb, 50 μM) and the EV-uptake inhibitor methyl-β-cyclodextrin (mβCD, 1 mM), but not by the inhibitor of exocytosis EXO1 (50 μM). In (*A*–*D*), the Z-dimension of each spheroid was scanned with an optical section thickness of 110 μm at an interval between sections of 10 μm. (Scale bar: 200 μm.) Images in the *Left* panels were quantified and the normalized mean fluorescence presented in the *Right* panels. (*E*) Confocal images of cryo-sectioned tumor tissues from HCT-8GFP xenograft mice treated with DiI/R/AD show the process of EV-mediated delivery in the tumor. The DiI fluorescence appeared in EVs derived from HCT-8GFP tumor (arrows). The hollow-donut shape of red DiI signal with green GFP filling highlights the HCT-8GFP-derived EVs with the DiI-labelled phospholipid bilayer and the HCT-8GFP-derived contents inside. Box 1, a DiI-loaded EV (arrow) located within the intercellular space; Box 2 to 4, the DiI-loaded EVs mediated intercellular transport within the tumor. Box 2, DiI-loaded EVs adhered onto the cell surface; Box 3, a DiI-loaded EV entering into a cell; Box 4, a DiI-loaded EV inside a cell. The tumor tissues were collected 24 h after intravenous injection of DiI/R/AD in HCT-8GFP xenografts.

Overcoming Side Effects of Drugs. It is important to note that ADNMs facilitated deep intratumoral delivery and achieved effective anticancer activity (Fig. 2) with no notable toxicity or side effects such as those normally associated with anticancer drugs. Indeed, the mice treated with ADNMs exhibited no abnormal behavior throughout the treatment period, and no significant weight loss was detected (*SI Appendix*, Fig. S1 *E–G*). In fact, slight weight gain was observed for the treated mice (*SI Appendix*, Fig. S1*G*). Considering that many anticancer drugs are limited by severe toxicity and side effects, this additional evidence of the excellent safety profile of ADNMs is extremely promising.

Specifically, the anticancer drug DOX is associated with cardiotoxicity, (52) while the immunosuppressive effect of R can promote tumor metastasis. (53) Remarkably, no visible heart tissue damage was observed in the DOX/AD treatment group, whereas mice treated with free DOX displayed hyperemia and myocardial fiber breakage (Fig. 6*A*). In addition, no metastasis was observed in HCT-8 xenograft mice treated with R/AD, whereas mice treated with free rapamycin exhibited significant lung metastasis (Fig. 6*B*). The markedly reduced toxicity and lack of side effects can be attributed to the preferential accumulation of ADNMs within the tumor via the EPR effect, and to the in situ tumor-secreted EV-mediated delivery. Notably, ADNMs enhanced the cellular uptake of EVs (Fig. 3 *K* and *L*), resulting in fewer tumor-derived EVs escaping and a consequentially reduced toxicity and pro-metastatic tendency of the tumor. Altogether, our results demonstrate that the ADNM-based DDS both effectively improved the therapeutic effects of anticancer drugs and greatly

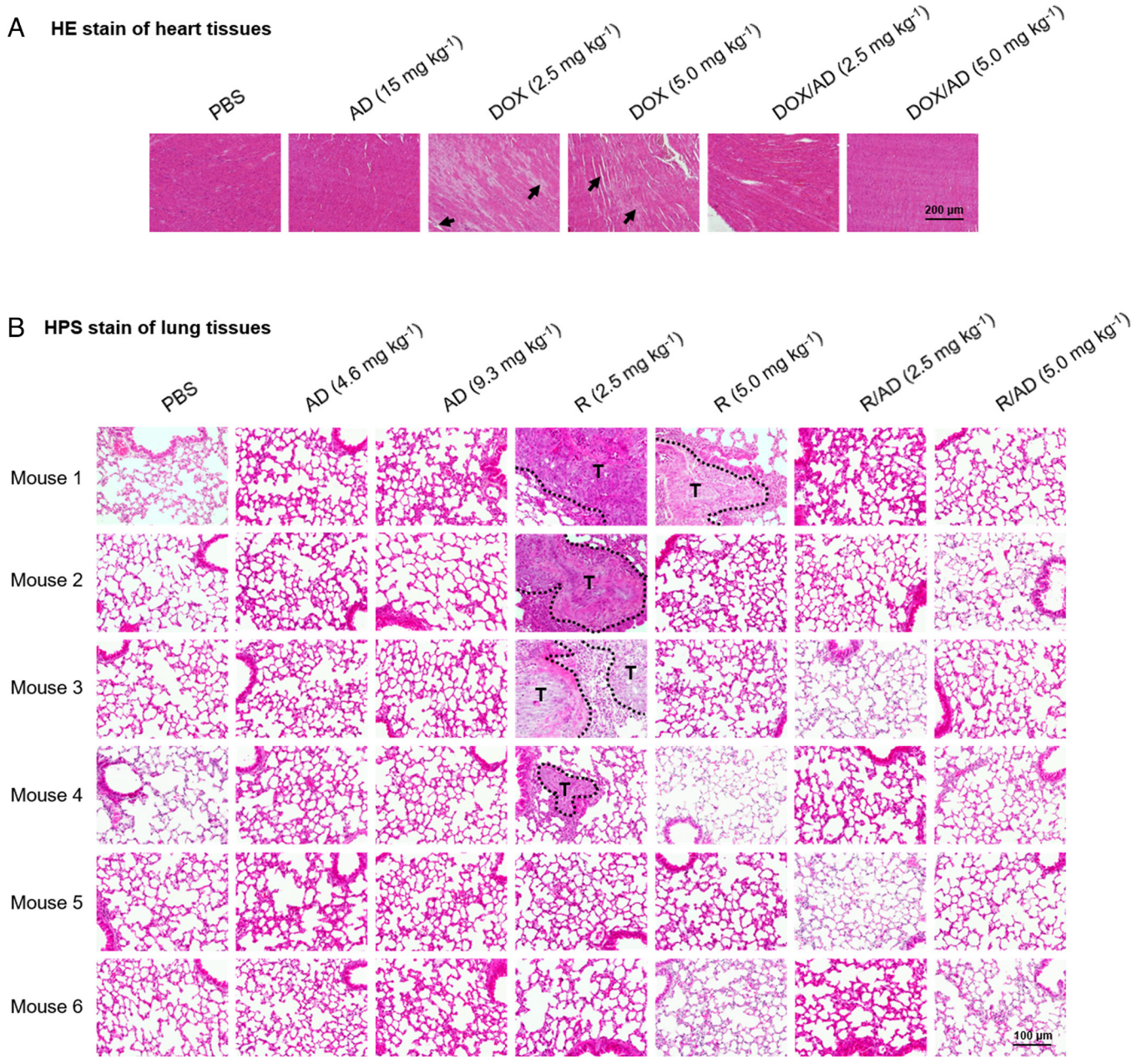

Fig. 6. ADNMs Reduced Drug Toxicity and Prevented Tumor Metastasis. (*A*) HE stain of heart tissue issued from PDAC087T xenografts treated with PBS, AD, DOX and DOX/AD (n = 6). Treatment with DOX/AD prevented DOX-induced hyperemia and myocardial fiber breakage (arrows) in heart. (*B*) HPS stain of lung tissues issued from HCT-8 xenografts treated with PBS, AD, R and R/AD (n = 6). Treatment with R/AD prevented the rapamycin-induced lung metastasis (T represents the tumor). Lung metastases were observed in mice treated with R, but not in those treated with PBS, dendrimer alone (AD) or the R/AD. Lung tissue was collected from mice at the end of treatment.

reduced their toxicity and related side effects via in situ-generated EV-mediated delivery.

Conclusion

In our search for DDSs that can overcome tumor heterogeneity and achieve deep tumor penetration, we have established ADNMs that promote and exploit in situ tumor-secreted EVs for effective delivery of their cargos. These ADNMs were able to encapsulate different anticancer drugs with high loading and encapsulating efficiency, and effectively accumulate within tumor lesions via the EPR effect. Upon tumor uptake, the payload of the ADNMs was repackaged into EVs by the parental cells. The secreted cargo-loaded EVs were further transported and internalized within the tumor that in turn relayed the drug to other cells. The cargo-loaded EVs and their cell-to-cell relay evolved according to the parental cells present within the TME, leading to adaptive drug delivery with deep intratumoral penetration. Consequently, ADNMs exhibited excellent anticancer activity in different models of both poorly and highly permeable tumors while simultaneously reducing the side effects and overcoming the limitations normally experienced with the anticancer drugs tested.

These promising results indicate the remarkable potential of ADNM-based DDSs for cancer treatment. Our study not only provides a new perspective on exploiting the intrinsic features of tumors in the design of adaptive DDSs capable of overcoming tumor heterogeneity and dynamic evolution, but also opens up a new avenue to explore in the engineering of novel functional materials in biomedical applications. We are actively working in this direction.

Materials and Methods

Preparation of dendrimer AD. The amphiphilic dendrimer AD was synthesized according to the method reported previously (24). ^{1}H NMR (400 MHz, CDCl3/CD3OD = 3/1): δ 7.54 (s, 1H), 4.17 (t, J = 4.0 Hz, 2H), 3.62 (s, 2H), 3.13–2.97 (m, 28H), 2.67–2.47 (m, 44H), 2.45–2.30 (m, 12H), 2.29–2.06 (m, 28H), 1.76–1.66 (m, 2H), 1.20–1.00 (m, 30H), 0.69 (t, J = 6.8 Hz, 3H). ^{13}C NMR (100 MHz, CD_3OD): δ 174.0, 173.6, 173.5, 143.6, 124.0, 53.4, 52.3, 50.2, 49.9, 49.3, 41.7, 41.5, 40.8, 37.4, 33.6, 31.9, 30.2, 29.6, 29.4, 29.3, 28.9, 26.4, 22.5, 13.3.

Preparation and Characterization of ADNMs. The drug- and/or dye-loaded ADNMs were prepared using the thin-film dispersion method (31). Typically, the payloads and AD were dissolved in the corresponding solvents separately, then mixed at the desired ratio. Specifically, the doxorubicin hydrochloride (DOX·HCl, Selleckchem) was dissolved in 1.0 mL of mixed solvent and neutralized with triethylamine [chloroform/methanol = 3/2 (v/v), DOX·HCl/triethylamine = 1/3 (mol/mol)], whereas, the rapamycin (R, Selleckchem) and paclitaxel (PTX, Selleckchem) were dissolved in 2.0 mL of methanol with or without dye such as Cy3 (Lumiprobe), DiI (ThermoFisher) and DiR (ThermoFisher), and then mixed with 3.0 mg of AD in 1.0 to 2.0 mL of methanol in a round bottom flask. Then the solvents were removed under reduced pressure to allow the formation of a thin film. Water (for DOX/AD) or 20 mM phosphate buffer [NaH_2PO_4 for R/AD and NaH_2PO_4/Na_2HPO_4 = 1/1 (mol/mol) for PTX/AD] was added into the flask and then gently shaken for hydration of the thin film (2.0 mL for 3.0 mg of AD). The so-formed micelle solutions were filtrated with 0.45-μm PTFE filter, followed by freezing and lyophilization. The lyophilized products were stored at −20 °C before use. The drugs encapsulated within the micelles were analyzed using high-performance liquid chromatography (HPLC, Waters) and the dyes were assessed using fluorescence spectrophotometer (Varian). The encapsulated drugs and dyes were quantified using standard curves, using the free drugs and dyes as reference standards.

Primary Pancreatic Cancer Cells. Primary cells were obtained from tumors from patients or patient-derived xenografts (PDX). Consent forms were collected from informed patients and recorded in a central database. The experimental procedure relating to the use of patient-derived pancreatic tumors was performed after approval from the South Mediterranean Personal Protection Committee, under the reference 2011-A01439-32. Expert clinical centers collaborated on this project after approval from their respective ethics review board (approval number 11-61).

A full description of the *Materials and Methods* is provided in *SI Appendix, SI Materials and Methods*.

Data, Materials, and Software Availability. All study data are included in the article and/or *SI Appendix*.

ACKNOWLEDGMENTS. We thank Dr. Kheya Sengupta and Ahmed Abdelrahman for the fluorescent microscopic imaging of EVs, Dr. Pascale Zimmermann and Dr. Rania Ghossoub for the use of NTA, and Odile Gayet for the cell culture. This work was supported by the Ligue Nationale Contre le Cancer (EL2016, EL2021 LNCCLiP, L.P.; Z.L.), Fondation de Recherche Médicale (Y.J.), French National Research Agency under the framework of the ERA-NET EURONANOMED European Research projects "Target4cancer" (L.P.), "NANOGLIO" (L.P.), "NAN-4-TUM" (L.P.) and "iNANOGUN" (L.P.), EU H2020 Research and Innovation program NMBP "SAFE-N-MEDTECH" (2019-2023) (grant agreement No. 814607, L.P., X.-J.L., B.R., T.R.), Campus France PHC CAI YUAN PEI program (L.P., X.-J.L.), and China Scholarship Council (L.D., J.L.).

Author affiliations: [a]Aix Marseille Université, CNRS, Centre Interdisciplinaire de Nanoscience de Marseille, UMR 7325, Equipe Labellisée Ligue Contre le Cancer, Marseille, 13288 France; [b]Centre de Recherche en Cancérologie de Marseille, INSERM U1068, CNRS, UMR 7258, Institut Paoli-Calmettes, Aix Marseille Université, 13273 Marseille, France; [c]Chinese Academy of Sciences (CAS) Key Laboratory for Biomedical Effects of Nanomaterials and Nanosafety, National Center for Nanoscience and Technology of China, 100190 Beijing, China; [d]University of Chinese Academy of Sciences, 100049 Beijing, China; and [e]Aix Marseille Université, CNRS, Mediterranean Institute of Microbiology, FR3479, 13009 Marseille, France

1. M. J. Mitchell *et al.*, Engineering precision nanoparticles for drug delivery. *Nat. Rev. Drug. Discov.* **20**, 101–124 (2021).
2. N. M. Anderson, M. C. Simon, The tumor microenvironment. *Curr. Biol.* **30**, R921–R925 (2020).
3. M. W. Dewhirst, T. W. Secomb, Transport of drugs from blood vessels to tumor tissue. *Nat. Rev. Cancer* **17**, 738–750 (2017).
4. I. Dagogo-Jack, A. T. Shaw, Tumor heterogeneity and resistance to cancer therapies. *Nat. Rev. Clin. Oncol.* **15**, 81–94 (2018).
5. M. Egeblad, E. S. Nakasone, Z. Werb, Tumors as organs: Complex tissues that interface with the entire organism. *Dev. Cell* **18**, 884–901 (2010).
6. I. Vitale, E. Shema, S. Loi, L. Galluzzi, Intratumoral heterogeneity in cancer progression and response to immunotherapy. *Nat. Med.* **27**, 212–224 (2021).
7. G. van Niel, G. D'Angelo, G. Raposo, Shedding light on the cell biology of extracellular vesicles. *Nat. Rev. Mol. Cell Biol.* **19**, 213–228 (2018).
8. I. K. Herrmann, M. J. A. Wood, G. Fuhrmann, Extracellular vesicles as a next-generation drug delivery platform. *Nat. Nanotechnol.* **16**, 748–759 (2021).
9. G. Raposo, P. D. Stahl, Extracellular vesicles: A new communication paradigm? *Nat. Rev. Mol. Cell Biol.* **20**, 509–510 (2019).
10. R. Xu *et al.*, Extracellular vesicles in cancer - implications for future improvements in cancer care. *Nat. Rev. Clin. Oncol.* **15**, 617–638 (2018).
11. P. Kucharzewska *et al.*, Exosomes reflect the hypoxic status of glioma cells and mediate hypoxia-dependent activation of vascular cells during tumor development. *Proc. Natl. Acad. Sci. U.S.A.* **110**, 7312–7317 (2013).
12. A. Moller, R. J. Lobb, The evolving translational potential of small extracellular vesicles in cancer. *Nat. Rev. Cancer* **20**, 697–709 (2020).
13. S. Lenzini, R. Bargi, G. Chung, J. W. Shin, Matrix mechanics and water permeation regulate extracellular vesicle transport. *Nat. Nanotechnol.* **15**, 217–223 (2020).
14. M. R. Muhsin-Sharafaldine, A. D. McLellan, Tumor-derived apoptotic vesicles: With death they do part. *Front. Immunol.* **9**, 957 (2018).
15. R. M. Kannan, E. Nance, S. Kannan, D. A. Tomalia, Emerging concepts in dendrimer-based nanomedicine: from design principles to clinical applications. *J. Intern. Med.* **276**, 579–617 (2014).
16. A. R. Menjoge, R. M. Kannan, D. A. Tomalia, Dendrimer-based drug and imaging conjugates: Design considerations for nanomedical applications. *Drug. Discov. Today* **15**, 171–185 (2010).
17. J. Lim, E. E. Simanek, Triazine dendrimers as drug delivery systems: From synthesis to therapy. *Adv. Drug. Deliv. Rev.* **64**, 826–835 (2012).
18. M. Malkoch, S. G. Gallego, *Dendrimer Chemistry: Synthetic Approaches Towards Complex Architectures* (Royal Society of Chemistry, 2020).
19. V. Percec *et al.*, Self-assembly of Janus dendrimers into uniform dendrimersomes and other complex architectures. *Science* **328**, 1009–1014 (2010).
20. S. E. Sherman, Q. Xiao, V. Percec, Mimicking complex biological membranes and their programmable glycan ligands with dendrimersomes and glycodendrimersomes. *Chem. Rev.* **117**, 6538–6631 (2017).
21. Z. Lyu, L. Ding, A. Tintaru, L. Peng, Self-assembling supramolecular dendrimers for biomedical applications: Lessons learned from poly(amidoamine) dendrimers. *Acc. Chem. Res.* **53**, 2936–2949 (2020).

22. J. Chen, D. Zhu, X. Liu, L. Peng, Amphiphilic dendrimer vectors for RNA delivery: State-of-the-art and future perspective. *Acc. Mater. Res.* **3**, 484–497 (2022).
23. M. Peterca, V. Percec, P. Leowanawat, A. Bertin, Predicting the size and properties of dendrimersomes from the lamellar structure of their amphiphilic Janus dendrimers. *J. Am. Chem. Soc.* **133**, 20507–20520 (2011).
24. T. Yu *et al.*, An amphiphilic dendrimer for effective delivery of small interfering RNA and gene silencing in vitro and in vivo. *Angew. Chem. Int. Ed. Engl.* **51**, 8478–8484 (2012).
25. V. Percec *et al.*, Modular synthesis of amphiphilic Janus glycodendrimers and their self-assembly into glycodendrimersomes and other complex architectures with bioactivity to biomedically relevant lectins. *J. Am. Chem. Soc.* **135**, 9055–9077 (2013).
26. X. Liu *et al.*, Adaptive amphiphilic dendrimer-based nanoassemblies as robust and versatile siRNA delivery systems. *Angew. Chem. Int. Ed Engl.* **53**, 11822–11827 (2014).
27. D. Dhumal *et al.*, An ionizable supramolecular dendrimer nanosystem for effective siRNA delivery with a favorable safety profile. *Nano Res.* **14**, 2247–2254 (2021).
28. D. Zhang *et al.*, One-component multifunctional sequence-defined ionizable amphiphilic Janus dendrimer delivery systems for mRNA. *J. Am. Chem. Soc.* **143**, 12315–12327 (2021).
29. D. Zhang *et al.*, Targeted delivery of mRNA with one-component ionizable amphiphilic Janus dendrimers. *J. Am. Chem. Soc.* **143**, 17975–17982 (2021).
30. D. Zhang *et al.*, The unexpected importance of the primary structure of the hydrophobic part of one-component ionizable amphiphilic Janus dendrimers in targeted mRNA delivery activity. *J. Am. Chem. Soc.* **144**, 4746–4753 (2022).
31. T. Wei *et al.*, Anticancer drug nanomicelles formed by self-assembling amphiphilic dendrimer to combat cancer drug resistance. *Proc. Natl. Acad. Sci. U.S.A.* **112**, 2978–2983 (2015).
32. J. Liu *et al.*, *Dendrimeric Nanosystem Consistently Circumvents Heterogeneous Drug Response and Resistance in Pancreatic Cancer. Exploration* (Wiley Online Library, 2021) pp. 21–34.
33. Y. Liu *et al.*, Biphasic rapamycin effects in lymphoma and carcinoma treatment. *Cancer Res.* **77**, 520–531 (2017).
34. Y. Matsumura, H. Maeda, A new concept for macromolecular therapeutics in cancer chemotherapy: Mechanism of tumoritropic accumulation of proteins and the antitumor agent smancs. *Cancer Res.* **46**, 6387–6392 (1986).
35. H. Maeda, J. Wu, T. Sawa, Y. Matsumura, K. Hori, Tumor vascular permeability and the EPR effect in macromolecular therapeutics: A review. *J. Control Release* **65**, 271–284 (2000).
36. Y. Shi, R. van der Meel, X. Chen, T. Lammers, The EPR effect and beyond: Strategies to improve tumor targeting and cancer nanomedicine treatment efficacy. *Theranostics* **10**, 7921–7924 (2020).
37. H. Cabral *et al.*, Accumulation of sub-100 nm polymeric micelles in poorly permeable tumors depends on size. *Nat. Nanotechnol.* **6**, 815–823 (2011).
38. X. Xie *et al.*, Eliminating blood oncogenic exosomes into the small intestine with aptamer-functionalized nanoparticles. *Nat. Commun.* **10**, 5476 (2019).
39. X. Wu *et al.*, Extracellular vesicles mediate the intercellular exchange of nanoparticles. *Adv. Sci.* **9**, e2102441 (2022).
40. F. Pi *et al.*, Nanoparticle orientation to control RNA loading and ligand display on extracellular vesicles for cancer regression. *Nat. Nanotechnol.* **13**, 82–89 (2018).
41. S. L. N. Maas, X. O. Breakefield, A. M. Weaver, Extracellular vesicles: Unique intercellular delivery vehicles. *Trends Cell Biol.* **27**, 172–188 (2017).
42. B. Wang *et al.*, Sequential intercellular delivery nanosystem for enhancing ROS-induced antitumor therapy. *Nano Lett.* **19**, 3505–3518 (2019).
43. J. Kowal *et al.*, Proteomic comparison defines novel markers to characterize heterogeneous populations of extracellular vesicle subtypes. *Proc. Natl. Acad. Sci. U.S.A.* **113**, E968–977 (2016).
44. G. K. Atkin-Smith *et al.*, Isolation of cell type-specific apoptotic bodies by fluorescence-activated cell sorting. *Sci. Rep.* **7**, 39846 (2017).
45. G. K. Atkin-Smith *et al.*, A novel mechanism of generating extracellular vesicles during apoptosis via a beads-on-a-string membrane structure. *Nat. Commun.* **6**, 7439 (2015).
46. H. Costa Verdera, J. J. Gitz-Francois, R. M. Schiffelers, P. Vader, Cellular uptake of extracellular vesicles is mediated by clathrin-independent endocytosis and macropinocytosis. *J. Control Release* **266**, 100–108 (2017).
47. V. Muralidharan-Chari *et al.*, ARF6-regulated shedding of tumor cell-derived plasma membrane microvesicles. *Curr. Biol.* **19**, 1875–1885 (2009).
48. E. Bielska *et al.*, Pathogen-derived extracellular vesicles mediate virulence in the fatal human pathogen Cryptococcus gattii. *Nat. Commun.* **9**, 1556 (2018).
49. Y. Feng *et al.*, Exo1: A new chemical inhibitor of the exocytic pathway. *Proc. Natl. Acad. Sci. U.S.A.* **100**, 6469–6474 (2003).
50. A. Zomer *et al.*, In vivo imaging reveals extracellular vesicle-mediated phenocopying of metastatic behavior. *Cell* **161**, 1046–1057 (2015).
51. C. Cheng, O. Trzcinski, L. C. Doering, Fluorescent labeling of dendritic spines in cell cultures with the carbocyanine dye "DiI". *Front. Neuroanat.* **8**, 30 (2014).
52. S. Raj, V. I. Franco, S. E. Lipshultz, Anthracycline-induced cardiotoxicity: A review of pathophysiology, diagnosis, and treatment. *Curr. Treat. Options Cardiovasc. Med.* **16**, 315 (2014).
53. T. J. Lin *et al.*, Rapamycin promotes mouse 4T1 tumor metastasis that can be reversed by a dendritic cell-based vaccine. *PLoS One* **10**, e0138335 (2015).